The Open Biotechnology Journal
Supplementary Material

Content list available at: https://openbiotechnologyjournal.com

Intralipid-Based Phantoms for the Development of New Optical Diagnostic Techniques

Maria Lepore[1] and Ines Delfino[2,*]

[1]*Dipartimento di Medicina Sperimentale, Università "Luigi Vanvitelli", Napoli, Italy*
[2]*Dipartimento di Scienze Ecologiche e Biologiche, Università della Tuscia, Viterbo, Italy*

Article History	Received: September 03, 2019	Revised: October 17, 2019	Accepted: October 26, 2019

SUPPLEMENTARY TABLES AND FIGURES

1) Time-resolved transmittance and reflectance: theoretical description

Light propagation in turbid media is usually described using diffusion equation:

$$\frac{1}{c}\frac{\partial}{\partial t}\phi - D\nabla^2\phi(\vec{r},t) + \mu_a\phi(\vec{r},t) = S\phi(\vec{r},t) \quad (1) \qquad \textbf{(1)}$$

where $\phi(\mathbf{r}, t)$ is the photon flux, D is the diffusion coefficient and $S(\mathbf{r}, t)$ is the source term (usually assumed to be a δ-function). The most used analytical expressions for time-resolved transmittance (T_1) and reflectance (R_1) through a slab of thickness *d* are the following [S1]:

$$T_1(d,t) = (4\pi D_1 c)^{-1/2}(t-t_0)^{-3/2}\exp[-\mu_a c(t-t_0)]\times$$
$$\left\{(d-z_0)\exp\left[-\frac{(d-z_0)^2}{4D_1c(t-t_0)}\right] - (d+z_0)\exp\left[-\frac{(d+z_0)^2}{4D_1c(t-t_0)}\right] + \right.$$
$$\left.(3d-z_0)\exp\left[-\frac{(3d-z_0)^2}{4D_1c(t-t_0)}\right] - (d+z_0)\exp\left[-\frac{(3d+z_0)^2}{4D_1c(t-t_0)}\right]\right\} \qquad \textbf{(2)}$$

$$R_1(\rho,d,t) = (4\pi D_1 c)^{-3/2}(t-t_0)^{-5/2}\exp\left[-\mu_a c(t-t_0) - \frac{\rho^2}{4D_1c(t-t_0)}\right]\times$$
$$\left\{z_0\exp\left[-\frac{z_0^2}{4D_1c(t-t_0)}\right] - (2d-z_0)\exp\left[-\frac{(2d-z_0)^2}{4D_1c(t-t_0)}\right] + \right.$$
$$\left.(2d+z_0)\exp\left[-\frac{(2d+z_0)^2}{4D_1c(t-t_0)}\right]\right\} \qquad \textbf{(3)}$$

* Address correspondence to this author at Dipartimento di Scienze Ecologiche e Biologiche, Università della Tuscia, Viterbo, Italy; Tel: +39 0761357026; E-mail: delfino@unitus.it

where $D=1/[3(\mu_a+\mu_s')]$, $z=1/\mu_s'$, for $\mu_s' >> \mu_a$, ρ is the distance of the source-detector distance in reflectance measurements, $\rho^2 >> z^2$, and c is the speed of the light.

In order to obtain the values of optical coefficients μ_a and μ_s', a fitting procedure between the theoretical curve obtained by using Eq. 2 (or Eq.3 if reflectance measurements are performed) and the experimental data is performed. In Fig. (**S1**) a typical example of the results of this numerical analysis is shown in terms of experimental data and obtained fitted curve.

As far as concerns experimental set-up for time-resolved transmittance and reflectance measurements, they are mainly composed by an ultrafast laser source able to deliver picoseconds or hundreds of femtosecond pulses and a detector (streak camera or a photon counting system) enabling to follow the temporal behavior of pulses after their interaction with turbid media. In Fig. (**S2**), a typical experimental time-resolved transmittance set-up is reported. An argon laser (Coherent, Model SABRE 40) is used for pumping a mode-locked Ti:Sa laser (Coherent, Model MIRA 900DUAL) with pulse duration of 130 fs, repetition rate of 76MHz and average power of 1.5 W. The detector is a streak camera (Hamamatsu Photonics, Model C5680, S1-IR extended photocathode). A small part of the laser pulse is sent to a photodiode (Hamamatsu, Model C1808) to obtain the trigger signal for the streak camera. After this, the laser light is coupled to two different optical fibers, one for the reference beam and the other for the main beam. Neutral density filters are used to reduce the pulse energy both for triggering, reference and main beams. The light transmitted through the sample is collected with a fiber bundle whose size is properly designed to match the entrance slit of the streak camera. Curves representing light intensity as a function of time are obtained from a two-dimensional CCD. The full temporal window recorded by the streak camera was about 3 ns. For further details see Ref. [S2].

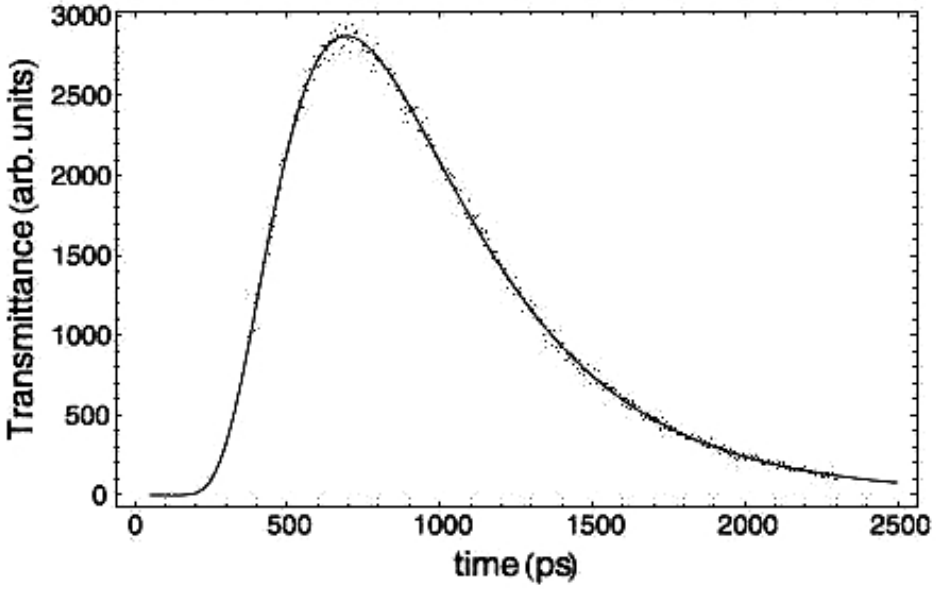

Fig. (S1). Time-resolved transmittance data (full circles) of the homogeneous phantom for a source–detector coaxial configuration. The fitting curve of the data (solid curve) is obtained by using the homogeneous solution of the diffusion equation; the calculated optical properties of the Intralipid solution are (μ'_s = 0.520±0.001 mm^{-1} and μ_a = (4.72±0.01)×10^{-3} mm^{-1}). Reprinted with permission from Esposito *et al* [S2]. Copyright 2004, Institute of Physics Publishing.

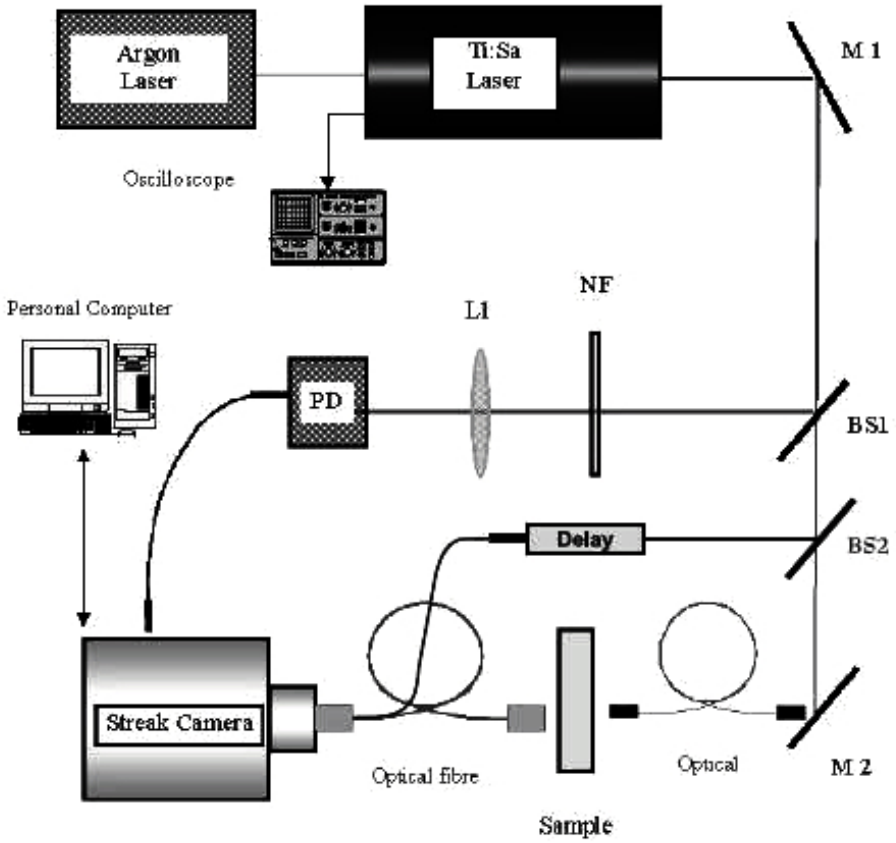

Fig. (S2). Typical experimental set-up for time-resolved transmittance measurements (M1, M2: mirrors, PD: photodiode, L1: lens, NF: neutral filters, BS1, BS2: beam splitters). Reprinted with permission from Esposito et al [S2]. Copyright 2004, Institute of Physics Publishing.

Absorbing Agents

When Intralipid is used for preparing phantoms that mimic the optical properties of human tissues different kinds of inks have to be used for adjusting the absorption coefficient. The most used ones are reported in Table **S1**. They are usually assumed purely absorbing even though some researchers noted that they also modify scattering properties of the prepared phantoms.

Table S1. List of the most largely used inks for preparation of phantoms and related references.

Commercial name	Refs.
India ink	[30], [31], [53], [57], [62], [S2], [S3],
Evans Blue	[46], [S4]
Cresyl blue	[62]
Greenish brown ink; Chugai Kasei Co., Musashino, Japan;	[S5]
Methylene Blue (M9140, Sigma- Aldrich, Missouri, USA)	[40], [41]

Hardener Substances

For preparing solid phantoms with Intralipid, hardener substances are required. These substances are expected do not alter the selected optical properties in a significant way, even though some authors noticed that some attention has to be paid to this aspect [53]. A list of the most used hardener substances is reported in Table **S2**. The various hardener substances that are used in Intralipid-based phantoms are selected depending on the specific application.

Table S2. List of the most largely used hardener for preparation of phantoms and related references.

Commercial name	Ref
Agar	[53], [S1], [S6]
Gelatin	[S7]-[S11]
Acrylamide	[58]

ADDITIONAL REFERENCES

[S1] Patterson MS, Chance B, Wilson BC. Time resolved reflectance and transmittance for the noninvasive measurement of tissue optical properties. Appl Opt 1989; 12(12): 2331-2336.

[S2] Esposito R, De Nicola S, Lepore M, Delfino I, Indovina PL. A perturbative approach to characterize absorptive inclusions in diffusing media by time-resolved contrast measurements. J. Pure & App. Phys. A 2004; 6: 736-741.

[S3] Wabnitz H, Jelzow A, Mazurenka M et al. Performance assessment of time-domain optical brain imagers, part 2: nEUROPt protocol. J Biomed Opt 2014; 19(8): 086012.

[S4] Zhang Y, Liu X, Wang Q, Liu D, Yang C, Sun J. Influence of extracerebral layers on estimates of optical properties with continuous wave near infrared spectroscopy: analysis based on multi-layered brain tissue architecture and Monte Carlo simulation. Computer Assisted Surgery 2019; 24(1): 144-150

[doi: 10.1080/24699322.2018.1557902]

[S5] Cook JR, Bouchard RR, Emelianov SY. Tissue-mimicking phantoms for photoacoustic and ultrasonic imaging. Biomed Opt Express 2011; 2 (11): 3193-3206.

[S6] Sato C, Shimada M, Yamada Y. Extraction of depth-dependent signals from time-resolved reflectance in layered turbid media. J Biomed Opt 2005; 10(6): 064008.

[S7] Krishnaswamy V, Michaelsen KE, Pogue BW, Poplack SP, Shaw I, Defrietas K, Brooks K, Paulsen KD. A digital x-ray tomosynthesis coupled near infrared spectral tomography system for dual modality breast imaging. Optics Express 2012; 20 (17): 19125-19136.

[S8] Lai P, Xu X, Wang LV. Dependence of optical scattering from Intralipid in gelatin-gel based tissue-mimicking phantoms on mixing temperature and time. J Biomed Opt 2014, 19(3), 035002.

[S9] Chen AI, Balter ML, Chen MI, Gross D, Alam SK, Maguire TJ, Yarmush ML. Multilayered tissue mimicking skin and vessel phantoms with tunable mechanical, optical, and acoustic properties. Medical Physics 2016; 43 (6): 3117-3131.

[S10] Cook JR, Bouchard RR, Emilianov SY. Tissue-mimicking phantoms for photoacoustic and ultrasonic imaging. Biomed Opt Express 2011; 2(11): 3193-3206.

[S11] Giller CA, Liu, H, Gurnani P, Victor S, Yazdani U, German DC. Validation of a near-infrared probe for detection of thin intracranial white matter structures. J Neurosurg. 2003; 98(6): 1299-1306.